In-situ electrosynthesis of hydrogen peroxide and wastewater treatment application: A novel strategy for graphite felt activation

Zhangweihao Pan[a], Kun Wang[a], Yi Wang[b,*], Panagiotis Tsiakaras[c,d,e], Shuqin Song[a]

[a] *The Key Lab of Low-carbon Chemistry & Energy Conservation of Guangdong Province, School of Materials Science and Engineering, Sun Yat-sen University, Guangzhou, 510275, PR China*
[b] *School of Chemical Engineering and Technology, Sun Yat-sen University, Zhuhai, 519082, PR China*
[c] *Laboratory of Electrochemical Devices based on Solid Oxide Proton Electrolytes, Institute of High Temperature Electrochemistry (RAS), Yekaterinburg, 620990, Russia*
[d] *Laboratory of materials and devices for electrochemical power industry, Ural Federal University, 19 Mira Str., Yekaterinburg, 620002, Russia*
[e] *Laboratory of Alternative Energy Conversion Systems, Department of Mechanical Engineering, School of Engineering, University of Thessaly, Pedion Areos, Volos383 34, Greece*

ABSTRACT

Electrochemical synthesis of hydrogen peroxide (H_2O_2) through O_2 electroreduction is an attractive alternative to the currently used anthraquinone process, and highly desirable for green chemical industries and environmental remediation. However, it remains a great challenge to develop cost-effective and durable electrocatalysts. Hence, rational strategy for developing electrocatalyst materials to achieve highly efficient 2e$^-$ pathway oxygen reduction reaction (ORR) electrocatalysis is extremely important for *in situ* electrochemical synthesis of H_2O_2.

In the present work, an economical activated graphite felt (AGF) material, following a simple and low-cost gaseous acetic acid activation method, is developed. With this activation process, the electrochemical performance of the AGF shows a great promotion for H_2O_2 production rate. Compared with raw graphite felt (RGF) material, the yield of H_2O_2 achieved on AGF is enhanced by several folds. The enhanced performance might be attributed to its specific pore structure, high content of defects and transformation of surface chemical bonds, which derives from the activation with gaseous acetic acid at high temperature.

It is found that the factors responsible for the remarkable electrocatalytic performance of AGF1100 are: 1) the special pore structure, which offers large area for reaction, obtained through gaseous acetic acid activation process at high temperature; 2) high content of sp^3−C bonds, defects, and oxygen-containing functional groups, which can act as active sites for oxygen adsorption or reduction during the electrocatalytic process.

1. Introduction

Hydrogen peroxide (H_2O_2), as an important industrial chemical, is widely used in many industrial fields, such as pulp and paper bleaching, wastewater treatment, chemical synthesis, metallurgy textile industry, electronic industry and so on [1]. However, up to now, H_2O_2 is generally and commonly produced through the anthraquinone oxidation process on an industrial scale, which is not only a high energy consumption process but also readily to cause environmental pollution [2]. So it is highly desirable to develop a mild, safe and economical method for H_2O_2 production, such as on-site direct synthesis [3], electrosynthesis [4], and photocatalytic synthesis [5].

Compared with the traditional anthraquinone oxidation process, H_2O_2 electrosynthesis has recently attracted more and more attention due to its lower energy consumption, higher yield and environmental

benignity [6]. As well-known, *oxygen reduction reaction* (ORR), as a significant electrochemical reaction, generally proceeds *via* 2e$^-$ or 4e$^-$ reaction pathways, and the product of 2e$^-$ ORR process is exactly H_2O_2 [7,8]. Unfortunately, due to its sluggish reaction kinetics [9], the electrocatalysts of this process still need to be developed. As in most of the already published literature reported [10,11], electrocatalysts with moderate defects as active sites to improve 2e$^-$ ORR selectivity and activity for efficient H_2O_2 performance were deservedly developed and adopted. These electrocatalysts are usually painted onto some three dimensional (3D) porous current collectors, such as *graphite felt* (GF) [12], carbon sponge [13] and carbon fiber [14], which are used as the cathodic ORR electrode for H_2O_2 accumulation. On the other hand, for this kind of painted electrodes, the adhesion between the catalysts and the current collector becomes weaker; this is due to the slow corrosion of the exterior catalyst during the long-term electrocatalytic process,

further leading to a poor stability. In addition, the use of polymer binder could block some catalytically active sites and further deteriorate the ORR activity. Typically, the *in-situ* construction or activation of the integrated 3D self-supported electrode could effectively address the above-mentioned issues as demonstrated in the succeeding sections as appropriate. Zhou et al. [15] reported that a GF cathode, which was *in-situ* modified with graphene by electrochemical exfoliation method, exhibited an ultrahigh yield of H_2O_2 production after optimizing the ratio of electrochemically exfoliated graphene and loading on the modified GF. Song et al. [16] developed a novel modified GF by the high-temperature KOH activation method, which demonstrated a considerable H_2O_2 yield of 79.2 mg L^{-1} at −0.7 V in 2 h. More importantly, the *in-situ* produced H_2O_2 was used to degrade various pollutants through the *electro-Fenton* (E-Fenton) process with excellent results. These pioneering works evoked great research interest in the *in-situ* activation of the integrated 3D self-supported electrode for the practical large-scale application of H_2O_2 electrosynthesis.

As of note, the moderate active sites of the modified electrode play a pivotal role in enhancing 2e⁻ ORR process. As an academic frontier, too many or highly-efficient active sites are not favorable for H_2O_2 generation, because in this case the ORR selectivity will evolve by the 4e⁻ pathway [17–21]. It is worthy pointing out that most reported N-doped carbon-based nanomaterials exhibit high 4e⁻ selectivity for ORR. This is because N-doping could effectively change the adsorption model of O_2, weakening in this way the O=O bonding energy and further improving their 4e⁻ ORR electrocatalytic performance [22]. However, some reported N-doped porous carbon materials identify high 2e⁻ selectivity to catalyze ORR [23–25], demonstrating that catalyst chemical structure also plays a vital role in determining its ORR selectivity. Moreover, with regard to undoped carbon materials, the morphology and pore structure are the key factors for H_2O_2 electrosynthesis. This could be attributed to the fact that appropriate morphology and pore structure could not only improve the rapid mass-transfer of H_2O_2 as intermediates, decreasing its residence time on the catalysts surface to avoid its further reduction, but also provide more accessible active sites for enhancing 2e⁻ ORR process. Quan et al. [26] reported that a novel hierarchically porous carbon possessed suitable defects (sp^3-C) as active sites and large specific surface area. Consequently, the optimized catalyst exhibited high 2e⁻ ORR selectivity in a wide pH range with high current efficiency. Recently, Cui et al. [27] found that the oxidized *carbon nanotubes* (CNT) exhibited higher 2e⁻ selectivity and better activity for ORR, whatever in basic or neutral media, compared with the original CNT. Experimental characterizations and density functional theory calculation showed that oxygen-containing functional groups in the oxidized CNT, mainly including −COOH and C−O−C, is propitious to enhancing 2e⁻ ORR process, whatever the onset potential or the H_2O_2 production rate. As always, it could be concluded that the O_2 adsorption energy of the catalysts has a typical volcano-type relationship with its H_2O_2 yield, which is mainly determined by the intensity of the active sites, including the

heteroatoms-doped and the intrinsic defects-induced ones. Very strong or weak O_2 adsorption of the catalysts could be unfavorable to the 2e⁻ ORR process.

In this work, an *in-situ activated graphite felt* (AGF), which is firstly formed through a simple and low-cost gaseous acetic acid activation method, is used for H_2O_2 electrosynthesis through ORR and wastewater treatment. As investigated, the smooth carbon fibers in the *raw GF* (RGF) becomes rough due to the strong etching effect exerted by the gaseous acetic acid at high temperature, further leading to the formation of abundant mesopores and defects. Also, the moderate active sites of the AGF, especially oxygen-containing functional groups, are obviously more than those of the RGF. As reported in the above section, either the pore structure or the active sites or both are favorable for the 2e⁻ ORR electrocatalytic process. Consequently, the AGF exhibited a high H_2O_2 generation rate with relatively low energy consumption, opening up a new way for developing efficient carbon-based cathodes.

2. Experimental method

2.1. Chemicals and materials

The commercial raw GF was obtained from Hunan-Jinhua Carbon High-tech Co. Ltd. All the other chemicals were purchased from Tianjindamao Reagent Corporation and used without further purification. All the used chemicals were of analytical grade.

2.2. GF activation

The commercial raw GF was immersed in acetone containing ultrasonic bath for 45 min in order to remove oily impurities, then rinsed with amounts of ethanol and deionized water, respectively, and finally dried in an oven at 60 °C for 12 h. After that, GF was annealed in N_2 atmosphere at different temperatures of 1000, 1100, and 1200 °C with a heating rate of 10 °C min⁻¹. When the temperature reached the target value, a stream of gaseous acetic acid, obtained by a liquid gasifying device, was immediately injected into the gas circuit system and maintained for 1 h; then it cooled down to room temperature with 10 °C min⁻¹. Finally, the sample was dried in a vacuum oven at 60 °C for 12 h. The detailed activation process is schematically seen in Fig. 1.

The commercial raw GF was marked as RGF, while the activated GF samples were denoted as AGF1000, AGF1100, and AGF1200, respectively (the number indicates the corresponding annealing temperature as described above).

2.3. Physico-chemical characterizations

Scanning electron microscopy (SEM) micrographs were taken by the aid of a LEO-1530VP microscope. *Transmission electron microscopy* (TEM) images were obtained by a FEI Tecnai G2 Spirit microscope. *X-ray photoelectron spectroscopy* (XPS) measurements were performed on
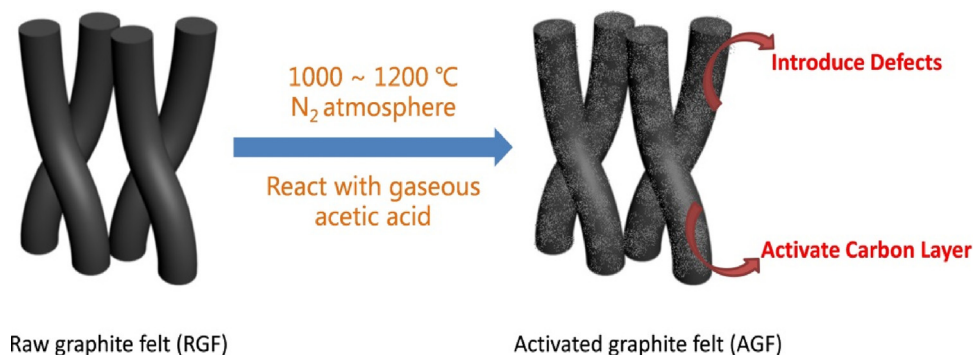

1000 ~ 1200 °C
N_2 atmosphere

React with gaseous acetic acid

Introduce Defects

Activate Carbon Layer

Raw graphite felt (RGF)

Activated graphite felt (AGF)

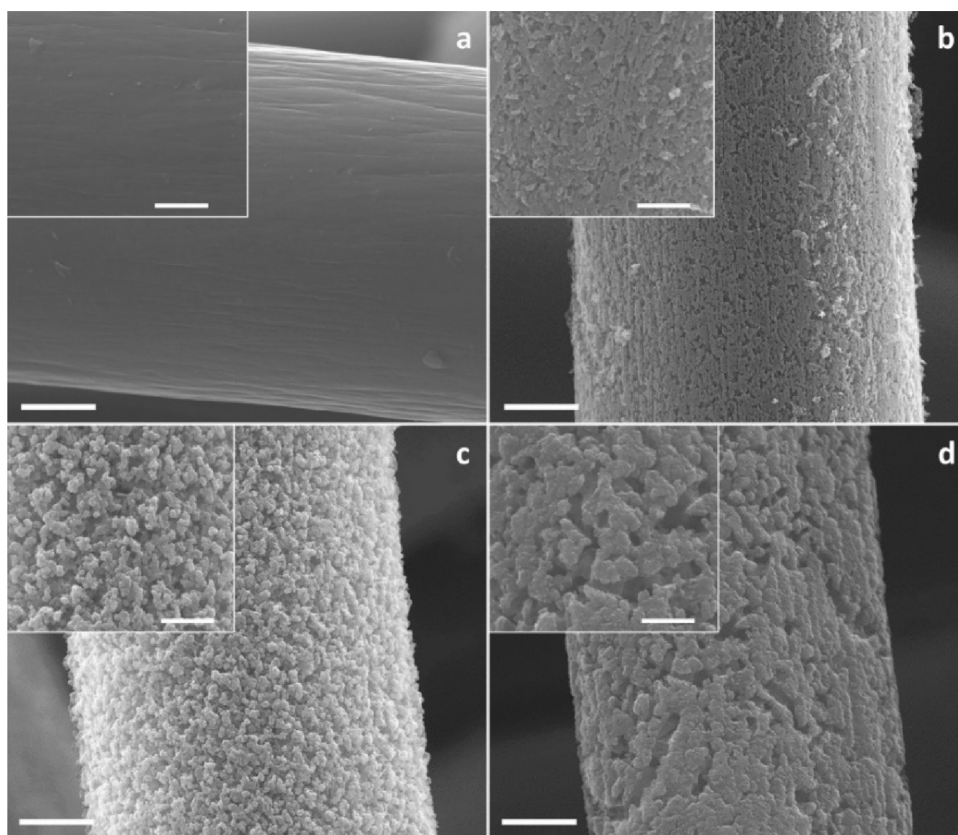**Fig. 1.** The schematic diagram of the activation process.

Fig. 2. The SEM images of RGF (a), AGF1000 (b), AGF1100 (c), and AGF1200 (d). (The bar in each image indicates 2 μm, while in inner image 1 μm).

an ESCALAB 250 spectrometer equipped with XR6 monochromatic X-ray source. N$_2$ adsorption & desorption experiments were carried out on Micromeritics ASAP 2460. The *Fourier transform infrared* (FT-IR) spectra were obtained using a Bruker EQUINOX 55 spectrograph. The Raman spectra were received by the aid of a HORIBA Jobin Yvon, LabRam HR800 laser co-focal micro-spectrometry spectrograph.

2.4. H$_2$O$_2$ accumulation and analysis

All electrochemical experiments were performed using a three-electrode system on Metrohm Autolab PGSTAT302 N station. RGF and AGF (AGF1000, AGF1100, and AGF1200) were used as the working electrode, while a graphite flake was used as the counter electrode. *Saturated calomel electrode* (SCE) and *Ag/AgCl electrode* (filled with saturated KCl solution) were used as the reference electrode in pH = 1.0 (0.05 M H$_2$SO$_4$ + 0.05 M Na$_2$SO$_4$), pH = 7.0 (0.05 M Na$_2$SO$_4$), and pH = 13.0 (0.1 M KOH) electrolytes, respectively. It should be noted that, for stability reasons, SCE was adopted in acidic and neutral electrolyte, while Ag/AgCl electrode was used in alkaline electrolyte. Accumulation of electrosynthetically produced H$_2$O$_2$ on the above working electrodes were performed in a two-compartment cell, using Nafion® 117 membrane as separator.

Both the cathode compartment (30 mL) and anode compartment were filled with the same electrolyte. During the H$_2$O$_2$ accumulation experiment, O$_2$ was bubbled by a glass tube into the solution at a flow rate of 0.6 L min^{-1} in order to keep the electrolyte saturated with O$_2$.

H$_2$O$_2$ concentration was detected by potassium-titanium oxalate method; the basis of this method is the formation of titanium(IV)-peroxide complex in the presence of sulfuric acid [28]. The detailed process of this method could be described as follows: a certain volume of the sample to be measured was added into the as-prepared potassium-

titanium oxalate K$_2$TiO(C$_2$O$_4$)$_2$ solution, and then the color of the solution changes into yellow because of the above chromogenic reaction. Next, the UV–vis technology was used to determine and calculate the content of the H$_2$O$_2$ in the samples.

For calculating the current efficiency of H$_2$O$_2$ electrosynthesis, the following equation was employed:

$$Current\ efficiency\ \% = \frac{nFCV}{Q} \times 100\%$$

Where n is the number of electrons needed for reducing oxygen to H$_2$O$_2$ (n = 2); F is the Faraday constant (96,485 C mol^{-1}); C is the H$_2$O$_2$ concentration (mol L^{-1}); V is the volume of electrolyte (L); Q is the amount of charge passed through the cell (C).

2.5. Applied for electro-fenton process

Among the various *in-situ* applications of direct electrochemical synthesis of H$_2$O$_2$ [16,24,29,30], an E-Fenton experiment for degrading pollutants was carried out as an example. Typically, conducted in a one-compartment cell, the RGF and AGF1100 (the optimized one as investigated) were set as the working electrode (active area of 0.5 cm^2); while graphite rod and SCE were served as anode and reference electrodes, respectively. Meanwhile, 40 mL of 5 mg L^{-1} *Rhodamine B* (RhB) was used as the target pollution, including 0.5 mM FeSO$_4$ and 0.05 M Na$_2$SO$_4$ as Fenton reagent and electrolyte, respectively. The solution pH value was adjusted to 3.0, using H$_2$SO$_4$. A constant potential was externally applied on the cathode during the E-Fenton process. For analyzing the degradation efficiency, a UV–vis spectrophotometer with absorption wavelength of 555 nm was used.

3. Results and discussion

3.1. Physico-chemical properties of GF

3.1.1. Morphology

The morphology of RGF and AGF was firstly investigated. As shown in Fig. 2, the SEM images reveal that the surface of RGF (Fig. 2a) is relatively smooth and with almost no defects. However, with the annealing temperature increasing, these morphological characteristics become increasingly rough. At 1000 °C (Fig. 2b), few cracks first appear on the surface, and then become denser and deeper with temperature rising.

After being annealed at 1100 °C, a uniformly porous structure on single GF fiber can be distinguished (Fig. 2c); this is due to the fact that exorbitant temperature of gaseous acetic acid treatment to the RGF could severely etch the surface the GF. As reported, these defects as active sites are favorable for enhancing ORR [26]. In addition, the as formed porous structure of AGF1100 could facilitate the rapid mass transfer of H_2O_2 and in this way avoid its further reduction into H_2O. But when the annealing temperature reaches 1200 °C, the result of etching becomes rude, which can be observed as rough surface in the case of AGF1200 (Fig. 2d), especially compared with those of AGF1000 and AGF1100. The same consequence can be obtained by TEM images (Fig. 3). Especially, it can be clearly seen that from the enlarged TEM images, AGF1000 still keeps the ordered layered structure (Inset of Fig. 3b), while AGF1200 has shown orderless structure, further indicating that 1100 °C is the suitable activation temperature.
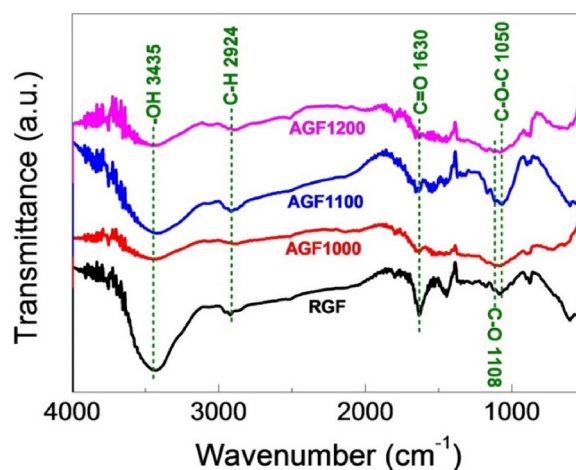

Fig. 4. The FT-IR spectra of RGF, AGF1000, AGF1100, and AGF1200.

Besides, reflected in a macroscopic scale, the structural stability of AGF1200 has broken, which means that it becomes crisp with no toughness. Therefore, AGF1200 could not stand up to the pressure of electrode holder while electrochemical testing; so that it is unpractical for actual use and this sample will not be further investigated in the electrochemical tests.
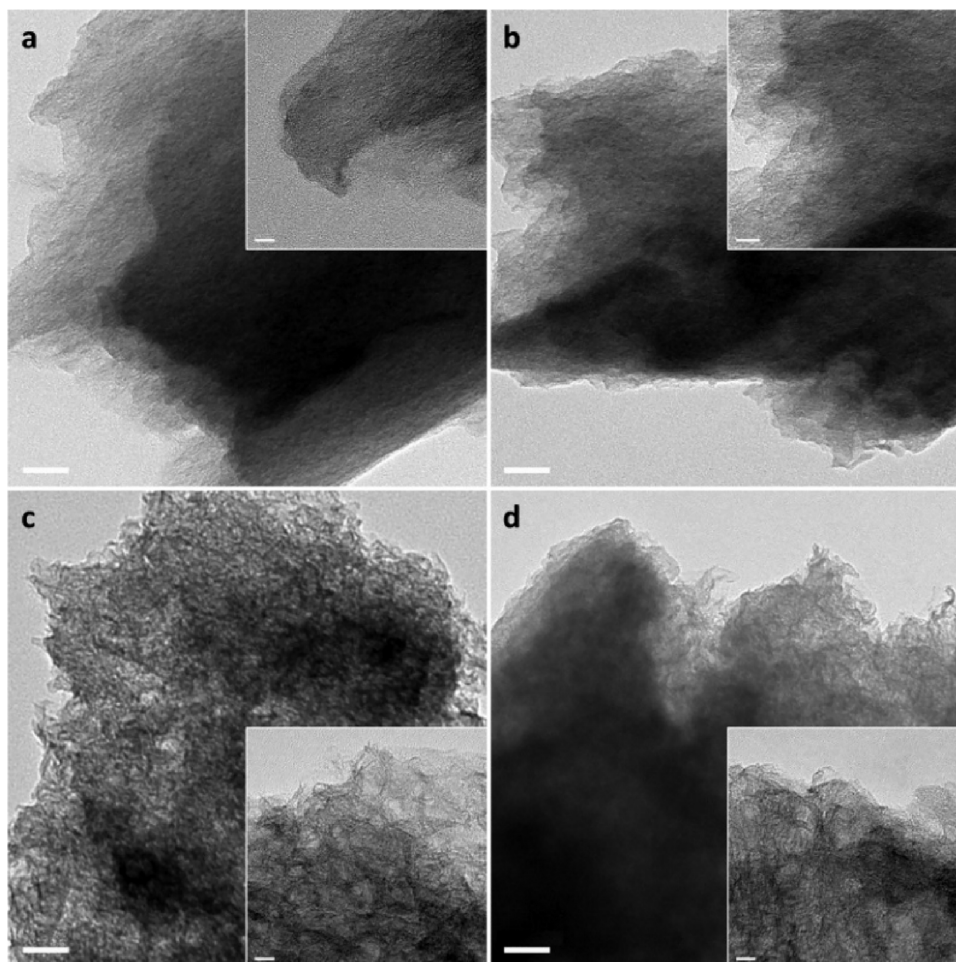

Fig. 3. The TEM images of RGF (a), AGF1000 (b), AGF1100 (c), and AGF1200 (d). (The bar in each image indicates 50 nm, while in inner image 10 nm).
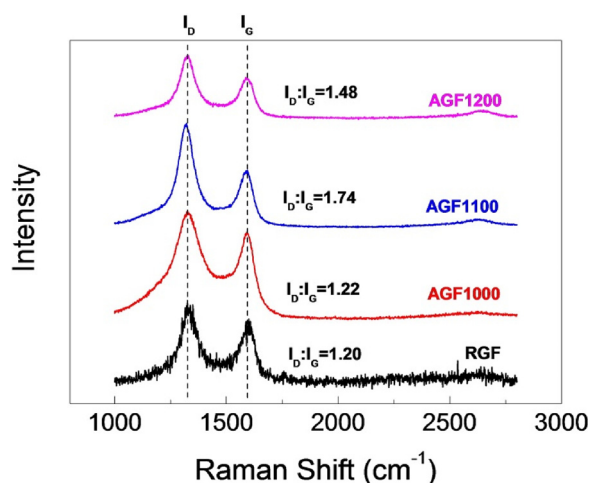
Fig. 5. The Raman spectra of RGF, AGF1000, AGF1100, and AGF1200.

3.1.2. FT-IR analysis

In the meantime, to investigate the chemical structures of the materials above, the vibrations of the groups were characterized by the FT-IR. As shown in Fig. 4. The bands at 3435 cm^{-1} and 1630 cm^{-1} are attributed to the vibrations of hydroxyl groups ($-OH$) axial deformation, and carbonyl groups ($-C=O$) stretching [31]. The small peak located at 2924 cm^{-1} can be assigned to the vibrations of -C-H bending and -C-H stretching [32].

Two bands at 1108 cm^{-1} and 1050 cm^{-1} originated from the oxygen-containing functional groups ($C-O$ and $C-O-C$), respectively [33], which could enhance the electrochemical performance of carbon materials and facilitate the H_2O_2 electrosynthesis [16].

3.1.3. Raman spectra analysis

To further identify the defects of the as prepared AGF, caused by the gaseous acetic acid activation process, Raman measurements were carried out. Fig. 5 shows the Raman spectra of RGF and AGF. The band located at ~1344 cm^{-1} corresponds to the disorder-induced band of the graphitic carbon (D band), while the one at ~1589 cm^{-1} represents the bond stretching of all pairs of the sp^2 carbon (G band) [26].

It can be seen that, during the annealing process, the intensity ratio ($I_D:I_G$) between peaks of D and G bands exhibits an escalating trend, which corroborates the surface defect formation reaction of GF, indicating that more defects are formed along with the annealing temperature increasing. This result is consistent with the SEM results, according to which the surface of the AGF-treated becomes rougher with respect to the original GF.

3.1.4. XPS analysis

In order to further understand the surface states of AGF, XPS was adopted to analyze their surface chemical bonds status. As presented in Fig. 6, for typical RGF and AGF1100 materials, peak fittings of C1s (Fig. 6a) and O1s (Fig. 6b) are carried out, and the relative contents of these surface groups of the samples are obtained by measuring the relative peak areas based on Fig. 6. The results are clearly listed in Table 1 and obviously indicate that these two elements have changed their states during the present activation process. For C1s spectra (Fig. 6a), the corresponding separated peaks are associated with C=C graphitized carbon (sp^2), C-C sp^3 carbon, C-O, C=O, and O=C-O [34]. It can be seen that sp^2 is transformed to sp^3 bonds after gaseous acetic acid activation at high temperature. It has been reported that sp^3 bonds of carbon materials can act as active sites for the reaction or adsorption during the electrocatalytic ORR process [26]. Both XPS and Raman results show that, the carbon content changes after gaseous acetic acid treatment. These sp^3 carbon and defects may promote the ORR and thereby facilitate H_2O_2 generation.
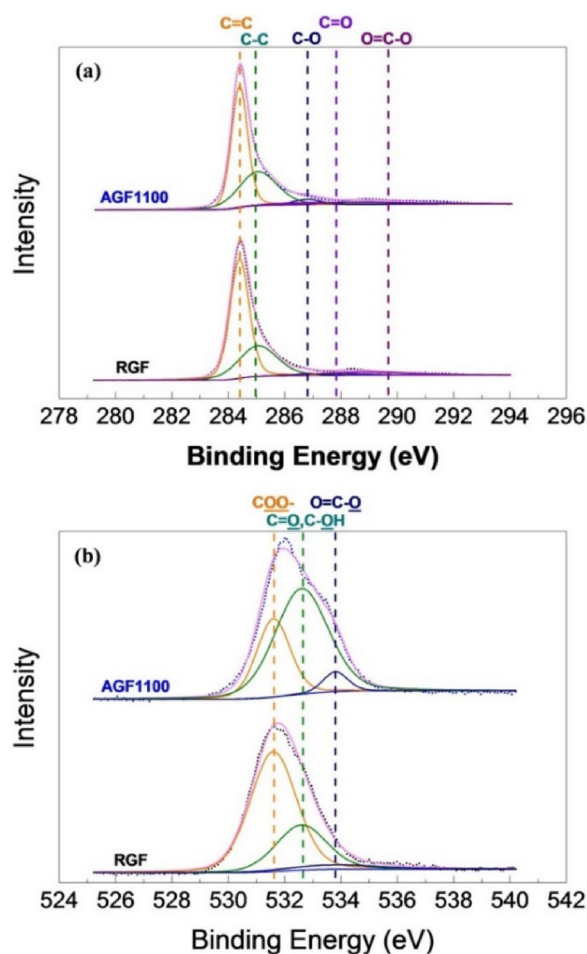

Fig. 6. The C1s (a) and O1s (b) XPS spectra of RGF and AGF1100.

Towards O1s spectra (Fig. 6b), regarding AGF1100, note worthily, the split peaks of C=O, C-OH, and O=C-O have increased after activation, while COO- has decreased. It is speculated that, during the activation process, COO- species have been converted into C=O, C-OH, and O=C-O, leading to the high catalytic activity [33].

These results show that oxygen-containing functional groups change could be caused by the gaseous acetic acid activation process at high temperature.

In addition, one can find that FTIR spectra show that the density of carboxyl groups (at 1630 cm^{-1}) are decreasing, but XPS data contradict. This is because the FTIR data are usually used for the qualitative analysis. It is meaningless to use the FTIR data to compare the content of certain specific oxygen functional groups for two different electrodes. However, the XPS characterizations are more credible for quantitative analysis.

3.1.5. N_2 adsorption & desorption experiment

For better understanding the microscopic structure, the pore structure of AGF was investigated by N_2 adsorption & desorption experiments. The results are shown in Fig. 7. It should be noted that, beyond the detection limit of absorbed N_2 quantity due to the smooth surface, the data of RGF are missed. During the activation process, the pore size distribution has changed. As seen in Fig. 7b, AGF1000 exhibits a wide pore size distribution, which ranges from 1 to 100 nm. For AGF1100, macropores and micropores have both increased from the surface of GF, which offers a remarkable reaction area. As the annealing temperature rises, the distribution of pore structure has become wide and disordered, demonstrating that activation process should be kept at a suitable temperature.

Table 1
The contents of carbon and oxygen-containing functional groups in RGF and AGF1100.

Sample			Carbon %					Oxygen-containing functional groups, %		
(eV)	C (%)	O (%)	C=C *(284.4)*	C–C *(285.0)*	C–O *(286.8)*	C=O *(287.8)*	O=C–O *(288.8)*	COO– *(531.4)*	C–OH, C=O *(532.6)*	O=C–O *(534)*
RGF	94.15	5.85	58.24	29.78	2.77	2.79	6.42	67.57	27.72	4.71
AGF1100	93.20	6.80	51.17	34.61	3.66	6.71	3.85	30.02	65.16	4.82

Those results announce that the activation process might go through a selective pore-making reaction and this process can reconstruct surface pore structure of GF. Moreover, the data of BET surface area and pore volume of the above materials listed in Table 2 also lead to the same conclusion.

3.2. Electrochemical performance of GF

3.2.1. Cyclic voltammetry (CV)

To explore the ORR activity of AGF, CV in N_2 and O_2-saturated solution was first evaluated in an electrolyte solution of pH = 1.0 (0.05 M H_2SO_4 + 0.05 M Na_2SO_4), which is presented in Fig. 8. As can be distinguished, a well-defined ORR current appears in the CV curves measured in O_2-saturated solution, whereas voltammograms without any noticeable peaks are obtained in N_2-saturated solution. This result indicates the pronounced ORR electrocatalytic activity of GF. The ORR onset potential of AGF1100 is close to 0.20 V, which is more positive than those of RGF (0.12 V), AGF1000 (0.14 V), and AGF1200 (0.16 V). Meanwhile, AGF1100 exhibits the biggest limited current. The results demonstrate that AGF1100 is more active for ORR than the others.

3.2.2. Rotating ring-disk electrode (RRDE) measurements

To further investigate the mechanism of the ORR at AGF, the RRDE measurements were collected in O_2-saturated pH = 1.0 solution for monitoring the selectivity of H_2O_2 production, by detecting the produced H_2O_2 by its quantitative oxidation at the Pt ring electrode [35]. According to the results shown in Fig. 9, ORR tends to undergo a $2e^-$ ORR pathway.

The selectivity of H_2O_2 production at AGF1100 reaches 60% between −0.2 and −0.8 V, indicating that a high yield of H_2O_2 is achievable. It is worth mentioning that the unusual change of n and H_2O_2% at negative potentials might be attributed to hydrogen evolution reaction, which, as a side reaction, could enhance the background current.

3.2.3. H_2O_2 accumulation experiments

In order to quantitatively analyze the H_2O_2 yield from $2e^-$ ORR, constant potential electrolysis was employed. Fig. 10 shows the plots of accumulated H_2O_2 concentration at GF *versus* electrolysis time and the

Table 2
The BET surface area and pore volume of RGF, AGF1000, AGF1100, and AGF1200.

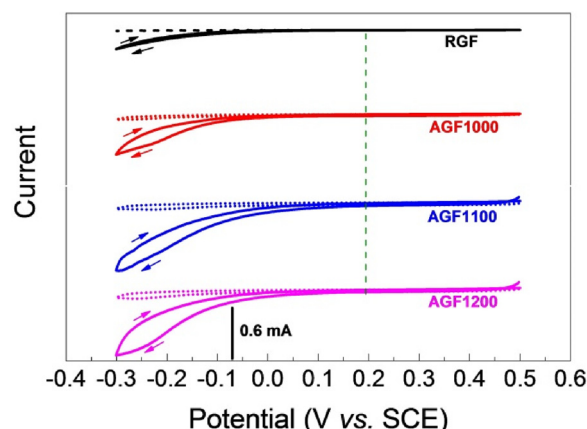| Sample	RGF	AGF1000	AGF1100	AGF1200
BET surface area (m² g⁻¹)	3.08	9.59	49.20	12.88
Pore volume (cm³ g⁻¹)	–	0.027	0.128	0.0567

Fig. 8. CV curves of RGF, AGF1000, AGF1100, and AGF1200 in N_2-saturated (dot line) and O_2-saturated (solid line) pH = 1.0 solution (0.05 M H_2SO_4 + 0.05 M Na_2SO_4) with a scan rate of 10 mV s⁻¹.

current efficiency are calculated and presented in the insets.

It can be obviously seen that, at all investigated GF electrodes, there is almost a linear accumulation of H_2O_2 over electrolysis time at - −0.3 V in pH = 1.0 electrolyte (Fig. 10a). These data clearly demonstrate that AGF1100 show the better performance of direct electrosynthesis of H_2O_2 *via* ORR compared with the RGF and AGF1000, which agrees well with the above reported results of CV and RRDE. The high performance of AGF1100 could be benefited from its following properties: i) suitable pore structure, ii) high-activity carbon content, iii) oxygen-containing functional groups, and iv) considerable surface area.
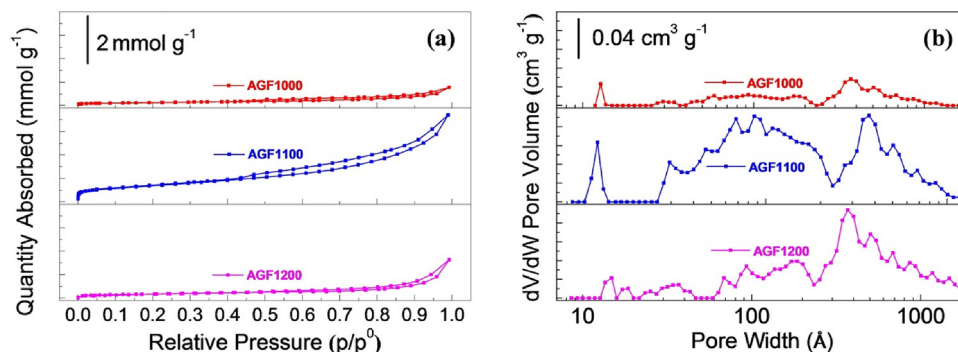

Fig. 7. N_2 adsorption & desorption curve (a) and pore size distribution (b) of AGF1000, AGF1100, and AGF1200.
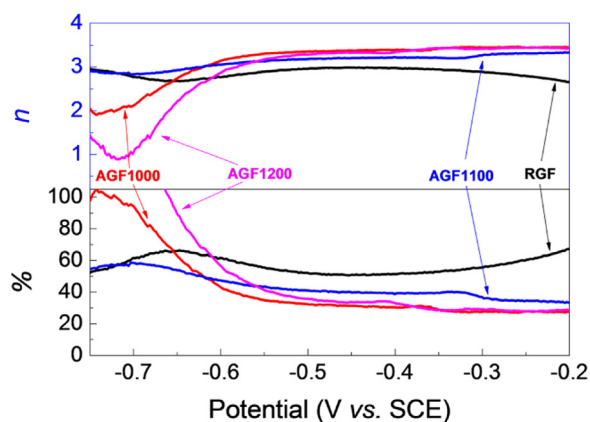
Fig. 9. RRDE results: calculated values of the average number of transferred electrons (n) in ORR process and H_2O_2 selectivity as a function of the applied potential.

The performance of AGF1100 for H_2O_2 synthesis was further evaluated in detail. Based on RRDE measurement results, the corresponding experimental conditions of H_2O_2 accumulation can be obtained. Fig. 10(b–c) show the accumulated H_2O_2 concentration at different potentials (in pH = 1.0 solution) and in different pH solutions (at -0.7 V); the corresponding current efficiencies are calculated and presented in the inset. It is worth noting that the H_2O_2 yield increases as the potential is negatively shifted in the investigated potential range. When O_2 is electrochemically reduced at AGF1100 at −0.7 V in the pH = 1.0 solution, the concentration of H_2O_2 produced within 1 h is close to 472.9 mg L^{-1}, with an acceptable current efficiency. This production rate is much higher than those obtained over recently reported electrocatalysts [23,36–39] under similar conditions (Table 3).

Besides, AGF1100 also exhibits good performance among acidic (472.9 mg L^{-1}), neutral (343.0 mg L^{-1}) and alkaline (385.2 mg L^{-1}) solutions, which still outperforms non-noble-metal electrocatalysts recently reported (Tables 4 and 5) [40–45].

Furthermore, the repeatedly H_2O_2 accumulation process was employed to investigate the stability of AGF1100. Under the condition of constant potential −0.7 V (*vs.* SCE) in a pH = 1.0 electrolyte, each process was lasted for 1 h. Before the process was repeated, the used AGF1100 electrode was cleaned with deionized water.

From Fig. 11, it can be distinguished that the final H_2O_2 accumulation concentration of each process ranges within an acceptable error, indicating that the activity of AGF1100 electrode is stable with time.

3.2.4. Pollutant degradation at AGF1100 in E-Fenton system

RhB, as a common dye, is widely used in laboratory and factory. However, it is hard to be degraded due to its high chemical stability. Therefore, RhB is a typical degradation target of E-Fenton process application. The comparative RhB degradation results at RGF and AGF1100 cathode through E-Fenton process are presented in Fig. 12.

It can be seen that, RhB can be completely degraded at AGF1100 within 15 min and the kinetic constant reaches ∼ 0.27 min^{-1}, while at RGF it takes 30 min with a kinetic constant of 0.11 min^{-1}. With the superior activity of AGF1100, the E-Fenton degradation efficiency is enhanced as well. All the results demonstrate that the AGF1100 is a promising E-Fenton cathode in wastewater treatment.

4. Conclusion

Based on the aforementioned results, the following factors are responsible for the remarkable electrocatalytic performance of AGF1100: 1) the special pore structure, which offers large area for reaction, has been obtained through the gaseous acetic acid activation procedure at high temperature and 2) the high content of sp^3-C bonds, defects, and
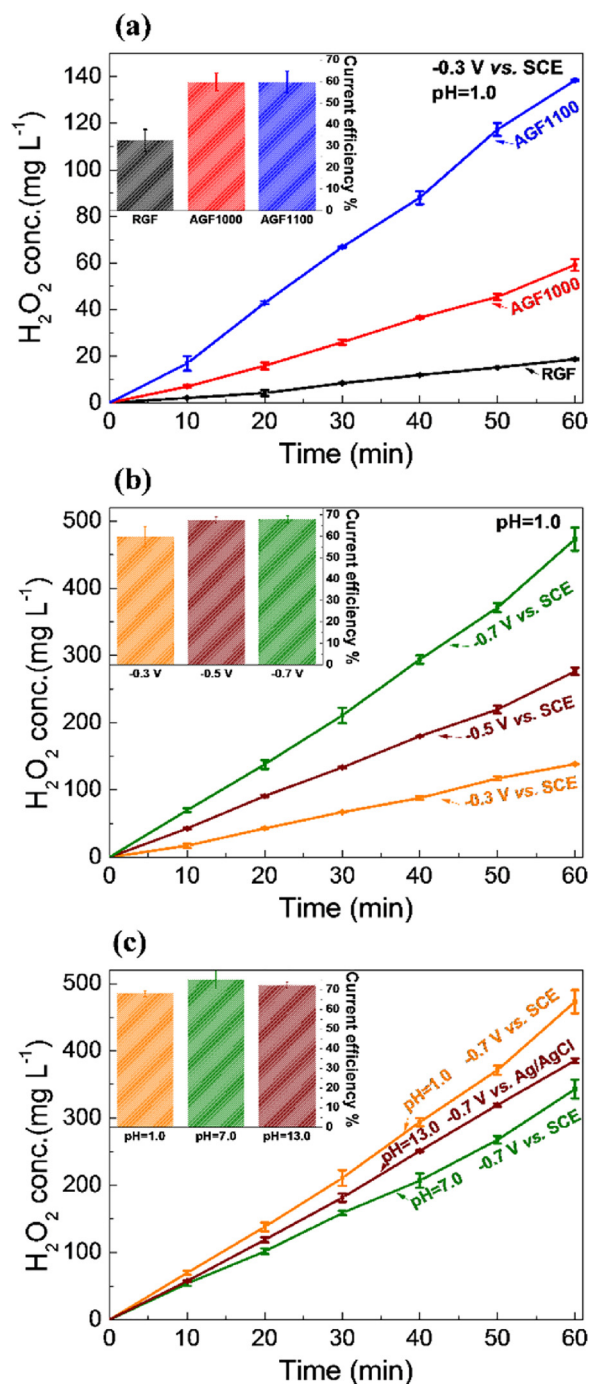

Fig. 10. H_2O_2 concentration measured by several accumulation conditions: (a) comparison of RGF, AGF1000 and AGF1100 in pH = 1.0 solution (0.05 M H_2SO_4 + 0.05 M Na_2SO_4); (b) testing of AGF1100 with several potentials in pH = 1.0 solution; (c) testing of AGF1100 in pH = 1.0 solution, pH = 7.0 solution (0.05 M Na_2SO_4) and pH = 13.0 solution (0.1 M KOH) with at -0.7 V.

oxygen-containing functional groups, which can act as reactive sites for oxygen adsorption or reduction during the electrocatalytic process.

For promoting *graphite felt* (GF) as an economical, stable and industrial electrode for the electrochemical synthesis of H_2O_2 through $2e^-$ ORR pathway, a novel, easy and highly effective chemical vapor reaction method for GF activation has been presented. Further characterizations such as SEM, TEM, Raman spectrum, FT-IR, XPS and N_2 adsorption & desorption results showed that pore structure and surface chemical state became more suitable for $2e^-$ ORR process after the activation process. The electrosynthesis of H_2O_2 was tested at typical

Table 3

Comparison of H_2O_2 accumulation concentration, production rate and current efficiency at pH = 0-1.

Sample	pH	Potential (V vs. RHE)	[H_2O_2] (mg L^{-1} h^{-1})	Efficiency (%)	Refs
N-doped porous carbon	1.0	0.10	3.3	65.2	[23]
Riboflavinyl-anthraquinone carboxylate ester/ XC72	0	0.10	21.0	70.0	[38]
Co/carbon	0	0.25	13.6	80.0	[36]
Anthraquinone/carbon black	0.7	−0.72	354.0	26.3	[39]
Carbon black with 5.0% FePc	0.7	−0.46	~120.0	–	[37]
AGF1100	1.0	−0.40	472.9	68.0	This work

Table 4

Comparison of H_2O_2 concentration, production rate and current efficiency at pH = 6~7.

| Sample	pH	Potential (V vs. SCE)	[H_2O_2] (mg L^{-1} h^{-1})	Efficiency (%)	Refs
Carbon fiber	7.0	−0.15	8.6	52.0	[42]
Modified graphite	7.0	−0.65	87.9	80.8	[43]
Carbon nanotube	6.0	−0.45	81.0	32.0	[44]
Anthraquinone-monosulphonate/ polypyrrole	6.3	−0.40	25.1	55.5	[45]
Co/carbon	7.0	−0.40	1.5	–	[36]
AGF1100	7.0	−0.70	343.0	75.3	This work

Table 5

Comparison of H_2O_2 concentration, production rate and current efficiency in pH = 13.0 solution.

Sample	pH	Potential (V vs. Ag/AgCl)	[H_2O_2] (mg L^{-1} h^{-1})	Efficiency (%)	Refs
CeO$_2$/C	13.0	−0.7	~100.0	44.0	[40]
Vulcan carbon	13.0	−0.7	~55.0	41.0	[40]
12% V/C	13.0	−0.7	~155.0	68.0	[41]
AGF1100	13.0	−0.7	385.2	72.3	This work

AGF1100 by applying voltage values ranging from −0.3 V to −0.7 V in acidic, alkaline, and neutral electrolyte, respectively. Under the above conditions, the obtained H_2O_2 yield was changed from 342.96 to 472.90 mg L^{-1} in 60 min, which is much higher than that obtained at commercial RGF. All these features indicate that this is an attractive activation process for the material using in direct electrochemical synthesis of H_2O_2 and it is also valuable for *in situ* utilization.

Through the electrochemical method, H_2O_2 can be *in situ* synthesized at moderate temperature and atmospheric pressure, avoiding the danger of explosion. With those advantages, direct electrochemical synthesis of H_2O_2 is a clean, economical, utilize-while-production
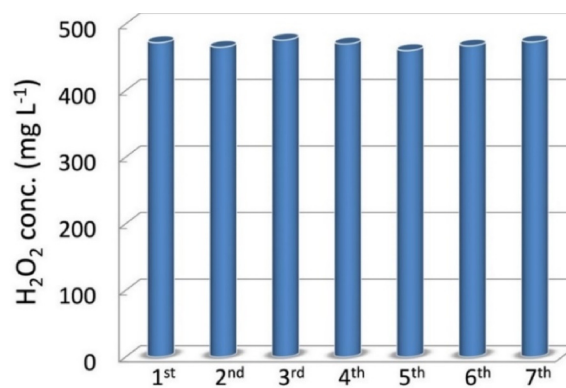
Fig. 11. Durability test for AGF1100.
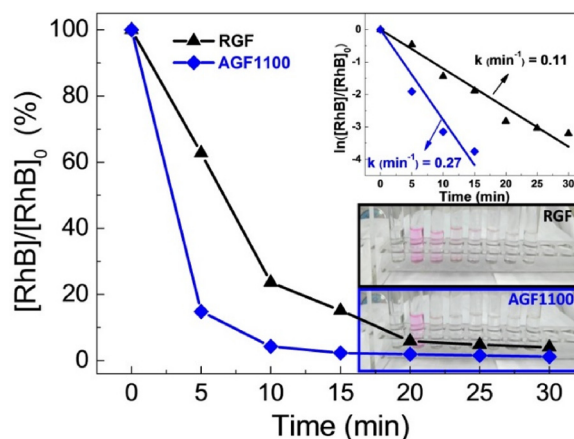
Fig. 12. RhB degradation efficiency, kinetics (inner plot) and phenomenon photograph of RGF and AGF1100.

technology; it can further be applied in various *in-situ* utilizing H_2O_2 scientific methods, such as E-Fenton process, drinking water purification, building energy-H_2O_2 cogeneration system by fuel cell and multi industry science.

Acknowledgements

References

[1] J.M. Campos-Martin, G. Blanco-Brieva, J.L. Fierro, Angew. Chem. Int. Ed. 45 (2006) 6962–6984.

[2] S.J. Freakley, Q. He, J.H. Harrhy, L. Lu, D.A. Crole, D.J. Morgan, E.N. Ntainjua, J.K. Edwards, A.F. Carley, A.Y. Borisevich, C.J. Kiely, G.J. Hutchings, Science 351 (2016) 965–968.

[3] L. Wang, S. Bao, J. Yi, F. He, Z. Mi, Appl. Catal. B: Environ. 79 (2008) 157–162.

[4] D.M. de Araújo, C. Sáez, C.A. Martínez-Huitle, P. Cañizares, M.A. Rodrigo, Appl. Catal. B: Environ. 166-167 (2015) 454–459.

[5] S. Zhao, T. Guo, X. Li, T. Xu, B. Yang, X. Zhao, Appl. Catal. B: Environ. 224 (2018) 725–732.

[6] I. Yamanaka, J. Jpn. Pet. Inst. 57 (2014) 237.
[7] L. Osmieri, R. Escudero-Cid, A.H.A. Monteverde Videla, P. Ocón, S. Specchia, Appl. Catal. B: Environ. 201 (2017) 253–265.
[8] M. Borghei, P. Kanninen, M. Lundahl, T. Susi, J. Sainio, I. Anoshkin, A. Nasibulin, T. Kallio, K. Tammeveski, E. Kauppinen, V. Ruiz, Appl. Catal. B: Environ. 158-159 (2014) 233–241.
[9] G. Zhang, Q. Wei, X. Yang, A.C. Tavares, S. Sun, Appl. Catal. B: Environ. 206 (2017) 115–126.
[10] X. Sheng, N. Daems, B. Geboes, M. Kurttepeli, S. Bals, T. Breugelmans, A. Hubin, I.F.J. Vankelecom, P.P. Pescarmona, Appl. Catal. B: Environ. 176-177 (2015) 212–224.
[11] M.B. Zakaria, C. Li, M. Pramanik, Y. Tsujimoto, M. Hu, V. Malgras, S. Tominaka, Y. Yamauchi, J. Mater. Chem. A 4 (2016) 9266–9274.
[12] J. Miao, H. Zhu, Y. Tang, Y. Chen, P. Wan, Chem. Eng. J. 250 (2014) 312–318.
[13] O. García-Rodríguez, J.A. Bañuelos, A. Rico-Zavala, L.A. Godínez, F.J. Rodríguez-Valadez, Int. J. Chem. React. Eng. 14 (2016) 843–850.
[14] G. Xia, Y. Lu, H. Xu, Electrochim. Acta 158 (2015) 390–396.
[15] W. Yang, M. Zhou, J. Cai, L. Liang, G. Ren, L. Jiang, J. Mater. Chem. A 5 (2017) 8070–8080.
[16] Y. Wang, Y. Liu, K. Wang, S. Song, P. Tsiakaras, H. Liu, Appl. Catal. B: Environ. 165 (2015) 360–368.
[17] T. Jiang, Y. Wang, K. Wang, Y. Liang, D. Wu, P. Tsiakaras, S. Song, Appl. Catal. B: Environ. 189 (2016) 1–11.
[18] Y. Hua, T. Jiang, K. Wang, M. Wu, S. Song, Y. Wang, P. Tsiakaras, Appl. Catal. B: Environ. 194 (2016) 202–208.
[19] Y. Wang, H. Liu, K. Wang, S. Song, P. Tsiakaras, Appl. Catal. B: Environ. 210 (2017) 57–66.
[20] K. Wan, G.-F. Long, M.-Y. Liu, L. Du, Z.-X. Liang, P. Tsiakaras, Appl. Catal. B: Environ. 165 (2015) 566–571.
[21] G. Liu, X. Li, P. Ganesan, B.N. Popov, Appl. Catal. B: Environ. 93 (2009) 156–165.
[22] K. Gong, F. Du, Z. Xia, M. Durstock, L. Dai, Science 323 (2009) 760–764.
[23] T.-P. Fellinger, F. Hasché, P. Strasser, M. Antonietti, J. Am. Chem. Soc. 134 (2012) 4072–4075.
[24] F. Hasché, M. Oezaslan, P. Strasser, T.-P. Fellinger, J. Energy Chem. 25 (2016) 251–257.
[25] Y. Yang, F. He, Y. Shen, X. Chen, H. Mei, S. Liu, Y. Zhang, Chem. Commun. 53 (2017) 9994–9997.
[26] Y. Liu, X. Quan, X. Fan, H. Wang, S. Chen, Angew. Chem. Int. Ed. 54 (2015)

6837–6841.
[27] Z. Lu, G. Chen, S. Siahrostami, Z. Chen, K. Liu, J. Xie, L. Liao, T. Wu, D. Lin, Y. Liu, T.F. Jaramillo, J.K. Nørskov, Y. Cui, Nat. Catal. 1 (2018) 156–162.
[28] Y. Sheng, S. Song, X. Wang, L. Song, Ch. Wang, H. Sun, X. Niu, Electrochim. Acta 56 (2011) 8651–8656.
[29] H. Zhao, Y. Chen, Q. Peng, Q. Wang, G. Zhao, Appl. Catal. B: Environ. 203 (2017) 127–137.
[30] Y. Liu, S. Chen, X. Quan, H. Yu, H. Zhao, Y. Zhang, Environ. Sci. Technol. 49 (2015) 13528–13533.
[31] M. Genovese, J. Jiang, K. Lian, N. Holm, J. Mater. Chem. A 3 (2015) 2903–2913.
[32] X. Wei, S. Wan, S. Gao, Nano Energy 28 (2016) 206–215.
[33] Z. Gao, F. Wang, J. Chang, D. Wu, X. Wang, X. Wang, F. Xu, S. Gao, K. Jiang, Electrochim. Acta 133 (2014) 325–334.
[34] Z. Liu, Z. Zhao, Y. Wang, S. Dou, D. Yan, D. Liu, Z. Xia, S. Wang, Adv. Mater. 29 (2017) 1606207.
[35] J.S. Jirkovský, I. Panas, E. Ahlberg, M. Halasa, S. Romani, D.J. Schiffrin, J. Am. Chem. Soc. 133 (2011) 19432–19441.
[36] A. Bonakdarpour, D. Esau, H. Cheng, A. Wang, E. Gyenge, D.P. Wilkinson, Electrochim. Acta 56 (2011) 9074–9081.
[37] F.L. Silva, R.M. Reis, W.R.P. Barros, R.S. Rocha, M.R.V. Lanza, J. Electroanal. Chem. 722-723 (2014) 32–37.
[38] A. Wang, A. Bonakdarpour, D.P. Wilkinson, E. Gyenge, Electrochim. Acta 66 (2012) 222–229.
[39] R.B. Valim, R.M. Reis, P.S. Castro, A.S. Lima, R.S. Rocha, M. Bertotti, M.R.V. Lanza, Carbon 61 (2013) 236–244.
[40] M.H.M.T. Assumpção, A. Moraes, R.F.B.D. Souza, I. Gaubeur, R.T.S. Oliveira, V.S. Antonin, G.R.P. Malpass, R.S. Rocha, M.L. Calegaro, M.R.V. Lanza, M.C. Santos, Appl. Catal. A: Gen. 411-412 (2012) 1–6.
[41] A. Moraes, M.H.M.T. Assumpção, R. Papai, I. Gaubeur, R.S. Rocha, R.M. Reis, M.L. Calegaro, M.R.V. Lanza, M.C. Santos, J. Electroanal. Chem. 719 (2014) 127–132.
[42] J. Choi, S.H. Hwang, J. Jang, J. Yoon, Electrochem. Commun. 30 (2013) 95–98.
[43] L. Zhou, M. Zhou, Z. Hu, Z. Bi, K.G. Serrano, Electrochim. Acta 140 (2014) 376–383.
[44] G. Gao, Q. Zhang, Z. Hao, C.D. Vecitis, Environ. Sci. Technol. 49 (2015) 2375–2383.
[45] G. Zhang, S. Wang, S. Zhao, L. Fu, G. Chen, F. Yang, Appl. Catal. B: Environ. 106 (2011) 370–378.